

Dust Penetrated Arm Classes: Insights from rising and falling rotation curves

M. S. Seigar^{1,2*}, D. L. Block³, I. Puerari⁴, N. E. Chorney^{2,5} and P. A. James⁶

¹*Department of Physics & Astronomy, University of California Irvine, 4129 Frederick Reines Hall, Irvine, CA 92697-4575, USA*

²*Joint Astronomy Centre, 660 N. A'ohoku Place, Hilo, HI 96720, USA*

³*School of Computational and Applied Mathematics, University of the Witwatersrand, P. O. Box 60, Wits, Gauteng 2050, South Africa*

⁴*Instituto Nacional de Astrofísica, Óptica y Electrónica, Apdo. Postal 51 y 216, 72000 Puebla, Pue., Mexico*

⁵*Department of Physics & Astronomy, University of Victoria, PO Box 3055 STN CSC, Victoria BC, V8W 3P6, Canada*

⁶*Astrophysics Research Institute, Liverpool John Moores University, Twelve Quays House, Egerton Wharf, Birkenhead CH41 1LD*

In original form 2004 October 3

ABSTRACT

In the last decade, near-infrared imaging has highlighted the decoupling of gaseous and old stellar disks: the morphologies of optical (Population I) tracers compared to the old stellar disk morphology, can be radically different. Galaxies which appear multi-armed and even flocculent in the optical may show significant Grand-Design spirals in the near-infrared. Furthermore, the optically determined Hubble classification scheme does not provide a sound way of classifying dust-penetrated stellar disks: spiral arm pitch angles (when measured in the near-infrared) do not correlate with Hubble type. The dust-penetrated classification scheme of Block & Puerari provides an alternative classification based on near-infrared morphology, and which is thus more closely linked to the dominant stellar mass component. Here we present near-infrared K band images of 14 galaxies, on which we have performed a Fourier analysis of the spiral structure in order to determine their near-infrared pitch angles and dust-penetrated arm classes. We have also used the rotation curve data of Mathewson et al to calculate the rates of shear in the stellar disks of these galaxies. We find a correlation between near-infrared pitch angle and rate of shear: galaxies with wide open arms (the γ class) are found to have rising rotation curves, while those with falling rotation curves belong to the tightly wound α bin. The major determinant of near-infrared spiral arm pitch angle is the distribution of matter within the galaxy concerned. The correlation reported in this study provides the physical basis underpinning spiral arm classes in the dust-penetrated regime and underscores earlier spectroscopic findings by Burstein and Rubin that Hubble type and mass distributions are unrelated.

Key words: Galaxies: fundamental parameters – Galaxies: spiral – Galaxies: structure – Infrared: galaxies

1 INTRODUCTION

The classification of galaxies by Hubble type (Hubble 1926), is traditionally inferred in the optical regime, where dust extinction still has a large affect, and where the light is dominated by the young Population I stars. Infrared arrays offer unique opportunities for decoupling the Population I and Population II disk morphologies, because in the K-band (2.2 μm), dust extinction is minimal, and the light is dominated by old and intermediate age stars (Rhoads 1998; Worthey 1994). The extinction at this wavelength is only 10% of that in the V-band (Martin & Whittet 1990).

Optically determined Hubble type is not correlated with dust-penetrated Population II morphology, as confirmed by the near-infrared studies of de Jong (1996) and Seigar & James (1998a, b). Even in the optical regime, the correlation between quantitative pitch angle and Hubble type is weak (see Kennicutt 1981), even though tightness of the spiral arm pattern, as judged by eye, is one of the defining Hubble morphological criteria. Furthermore, it has been shown that near-infrared morphologies of spiral galaxies can be significantly different from their optical morphologies (Block & Wainscoat 1991; Block et al. 1994a; Thornley 1996; Seigar & James 1998a, b; Seigar, Chorney & James 2003). Galaxies with flocculent spiral structure in the optical may present Grand-Design spiral structure in the near-infrared (Thorn-

* E-mail: mseigar@uci.edu (MSS)

ley 1996; Seigar et al. 2003). Such studies suggest that the optical morphology gives only incomplete and sometimes deceptive information about the underlying stellar mass distribution.

Burstein & Rubin (1985) showed that spiral galaxies can belong to one of three form families, based on the shapes of their rotation curves: whether rising, falling or flat. Burstein and Rubin differentiated three principal types of mass distribution and found that Hubble types Sa and Sb were represented amongst all three types in approximately equal numbers. This early spectroscopic study was a strong pointer to the decoupling of gaseous and stellar disks confirmed by near-infrared imaging.

From a dynamical viewpoint, the disk of a spiral galaxy can be separated into two distinct components: the *gas-dominated* Population I disk, and the *star-dominated* Population II disk. The former component contains features of spiral structure (OB associations, HII regions, and cold interstellar HI gas), which are naturally fast evolving; dynamically, it is very active and responsive, because, being characterized by small random motions (i.e. a ‘cool disk’), it fuels Jeans instability. In contrast, the Population II disk, which is dynamically ‘warmer’, contains the old stellar population highlighting the underlying stellar mass distribution (Lin 1971). One might expect, even in the absence of appreciable optical depths, for the two morphologies to be very different, since the near-infrared light comes predominantly from intermediate-age giant and supergiant stars (Rix & Rieke 1993; Frogel et al. 1996).

It is important to stress, that from this dynamical viewpoint, one requires two classification schemes, a near-infrared classification scheme, such as the dust-penetrated class (Block & Puerari 1999; Block et al. 1999) to describe the Population II disk, as well as optically determined Hubble type to describe the Population I disk. A near-infrared classification scheme can never replace an optical one, and vice-versa, because the current distribution of old stars strongly affects the distribution of gas in the Population I disk. The dynamic interplay between the two components (via a feedback mechanism) is crucial, and has been studied extensively (Bertin & Lin 1996). A central aspect here is the likely coupling of the Population I disk with that of the Population II disk via a feedback mechanism (Pfenniger et al. 1996). To derive a coherent physical framework for the excitation of spiral structure in galaxies, one must consider the co-existence of the two dynamical components.

There is a fundamental limit in predicting what evolved stellar disks might look like. The greater the degree of decoupling, the greater is the uncertainty. The fact that a spiral might be flocculent in the optical is very important, but it is equally important to know whether or not there is a decoupling with a Grand-Design old stellar disk. No prediction on that issue can, a priori, be made (Block, Elmegreen & Wainscoat 1996).

The theoretical framework to explain the co-existence of completely different morphologies within the same galaxy when studied optically and in the near-infrared is described by Bertin & Lin (1996), following the pioneering work of Lindblad (1963). A global mode (Bertin et al. 1989a, b) is composed of spiral wavetrains propagating radially in opposite directions, similar to a standing wave. Thus a feedback of wavetrains is required from the centre. The return

of wavetrains back to the corotation circle is guaranteed by refraction, either by the bulge or because the inner disk is dynamically warmer. In the stellar disk, such a feedback can be interrupted by the Inner Lindblad Resonance (ILR), which is a location where the stars meet the slower rotating density wave crests in resonance with their epicyclic frequency (Mark 1971; Lynden-Bell & Kalnajs 1972). In the gaseous disk, the related resonant absorption is only partial, so that some feedback is guaranteed. Once the above described wavecycle is set up (in the absence of a cutoff by an ILR), a self-excited global mode can be generated.

The tightness of the arms in the modal theory comes from the mass distribution and rate of shear. Galaxies with a more central mass concentration, i.e. higher overall densities (including dark matter) and higher rates of shear, are predicted to have more tightly wound arms. The models of Fuchs (1991, 2000) result in disks with rigidly rotating spiral modes, wherein bulges act as inner reflectors of waves or modes induced by the swing amplification method, thus leading to modal spiral waves, which form as a result of Toomre’s swing amplification (Toomre 1981). Fuchs (2000) adopts a stellar-dynamical analogue of the Goldreich & Lynden-Bell (1965) sheet, which describes the local dynamics of a patch of thin, differentially rotating stellar disk. The result is that, instead of shearing density waves (as in the unbounded sheet), spiral modes do appear. It can be shown that it is still the swing amplification mechanism, which is responsible for the appearance of the modes in these half-bounded disks. The models of Fuchs are disks which rigidly rotating spiral modes, wherein bulges act as inner reflectors of waves induced by swing amplification (see also Bertin & Lin 1996). These models best show how central mass concentration correlates with spiral arm pitch angle. If the disk is very light (low σ where σ is the disk density) the mode can be very tight, and one is in the domain of small epicycles (formally, the stability parameter $Q = c\kappa/\pi G\sigma$ being close to unity, the value of c must also be small, where c is the radial velocity dispersion and κ is the epicyclic frequency). If one increases the mass of the disk one finds a trend towards more open structures, but soon one runs the risk of a disk that is too heavy and a bar mode results. The trend towards more open spiral structure also follows a trend towards smaller rates of shear.

In those spirals with more open spiral arms at K but with no sign of a prominent bar, Bertin (1996) anticipates that the galaxy should be gas rich. Abundant gas can shock, dissipate and make some violently unstable open modes (Bertin & Lin 1996). This is one important reason why ‘gas content’ is important in the framework of modal theory for classification as the governing parameter for the trend from early-type (i.e. ‘a’) to late-type (i.e. ‘c’) spiral galaxies (Block et al. 1994a).

The redistribution of angular momentum by large-scale spiral torques will be stronger for stellar arms which are more open; some authors (eg. Pfenniger et al. 1996) have postulated that such a redistribution may lead to rapid changes in the disk with more mass being concentrated towards the centre, and even modify the properties of the rotation curve. This is the concept of secular evolution of a galaxy, from an open to a more tightly wound morphology, within one Hubble time.

Many galaxies show the presence of a significant $m=1$

component in the near-infrared (often in the form of a lopsidedness of the spiral). The linear modal theory predicts that $m=1$ modes should generally be dominated by $m=2$ modes when available, since the latter are more efficient in transporting angular momentum outwards. However, modes greater than $m=2$ are generally suppressed in the stellar disk by an ILR. While the disk mass participating in the mode is crucial, the gas-content of the galaxy is important: gas-rich spirals can generate modes greater than $m=2$. It had earlier been predicted (Block et al. 1994a, Bertin & Lin 1996) that infrared images should show an ubiquity of global one and two armed structures in the underlying stellar disk and the dust-penetrated classification scheme does confirm such a trend.

In contrast, the dynamics of the cold Population I gaseous disk, characterized by a different scalelength, velocity dispersion, thickness, and behaviour at the relevant Lindblad resonances, explains why spiral galaxies are optically so often overwhelmed by higher m modes and other more irregular fast evolving features, supported by the cold interstellar gas (Bertin 1991, 1993).

The dust-penetrated classification scheme (Block & Puerari 1999; Block et al. 1999) is a quantitative way of classifying galaxies according to their near-infrared spiral arm pitch angles (measured from $2 \mu\text{m}$ images). Details of this classification scheme are elucidated in section 3.

In this paper, we present near-infrared images for 14 spiral galaxies. We assign dust-penetrated classes to all of them and show that a correlation exists between the shear rate in stellar disks (as derived from their rotation curves) and their near-infrared spiral arm pitch angles. The dust penetrated arm class depends on the near-infrared spiral arm pitch angle, and so, such a correlation would provide a physical basis underpinning the dust penetrated arm scheme of Block & Puerari (1999). Section 2 describes the observations; section 3 describes our Fourier analysis and how we calculate pitch angles and assign dust penetrated classes; section 4 discusses our results and shows how we calculate shear rates in these galaxies while section 5 summarises our conclusions.

2 OBSERVATIONS

We have observed a sample of 14 galaxies in the near-infrared K-band ($2.2 \mu\text{m}$). These objects were taken from the study of Mathewson et al. (1992), who measured, by means of long-slit optical spectroscopy, $\text{H}\alpha$ rotation curves for 965 southern hemisphere spiral galaxies. Our sample includes galaxies with different rotation curve types (rising, falling and flat) and span as wide a range of optical Hubble types as possible. They were also chosen to have moderate inclination angles by restricting the ratio of the minor axis b to the major axis a using the range $0.50 < b/a < 0.66$. This results in values of inclination from $i \sim 42^\circ - 60^\circ$.

The images were observed at the United Kingdom Infrared Telescope (UKIRT) using the UKIRT Fast Track Imager (UFTI) between 1-4 August 2001, 11-12 March 2002 and 23 February 2004. The images from the August 2001 run were observed to a depth of $21.5 \text{ K-mag/arcsec}^2$ at the 3σ level, whereas those from the March 2002 and February 2004 runs were observed down to the same isophote, but at the 5σ level.

The galaxies observed in the August 2001 run were IC 1330, ESO 602-G25, ESO 606-G11, NGC 7677, UGC 14 and UGC 210. The galaxies observed in the March 2002 run were ESO 515-G3, ESO 574-G33, ESO 576-G51, ESO 583-G2, ESO 583-G7 NGC 2584 and NGC 2722. NGC 3456 was observed in February 2004. The sample is essentially the same as that of Seigar et al. (2003) with the addition of NGC 3456 (as it was observed at a later date) and the omission of ESO 543-G12, ESO 555-G8, ESO 576-G12 and UGC 12383, as reliable pitch angles could not be measured for these galaxies.

3 DECOMPOSITION AND IDENTIFICATION OF MODES

The 2-D Fast Fourier decomposition of all the near-infrared images in this study, employed a program developed by I. Puerari (Schröder et al. 1994). Logarithmic spirals are assumed in the decomposition.

The amplitude of each Fourier component is given by:

$$A(m, p) = \frac{\sum_{i=1}^I \sum_{j=1}^J I_{ij}(\ln r, \theta) \exp -(i(m\theta + p \ln r))}{\sum_{i=1}^I \sum_{j=1}^J I_{ij}(\ln r, \theta)} \quad (1)$$

where r and θ are polar coordinates, $I(\ln r, \theta)$ is the intensity at position $(\ln r, \theta)$, m represents the number of arms or modes, and p is the variable associated with the pitch angle P , defined by $\tan P = -\frac{m}{p_{max}}$. In this paper we measure the K-band pitch angle P_K of the $m=2$ component.

Our Fourier spectra corroborate earlier observational indications (Block et al. 1994a, 1999; Block & Puerari 1999) that there is indeed a ubiquity of $m=1$ and $m=2$ modes in the near-infrared. Block & Puerari (1999) proposed three principal archetypes for the evolved stellar disk of such galaxies. The first of these, designated dust-penetrated class α , covers the pitch angle range $4^\circ < P < 15^\circ$, the second, designated β , covers $18^\circ < P < 30^\circ$ and the third, designated γ covers $36^\circ < P < 76^\circ$.

Those galaxies where $m=1$ is the dominant mode are designated $\text{L}\alpha$, $\text{L}\beta$ and $\text{L}\gamma$ according to the dust penetrated pitch angle. Galaxies where $m=2$ is the dominant Fourier mode are classified into classes $\text{E}\alpha$, $\text{E}\beta$ and $\text{E}\gamma$. Higher order harmonics are classified as H3 (for $m=3$) and H4 (for $m=4$).

The range of radii over which the Fourier fits were applied are selected to exclude the bulge or bar (where there is no information about the arms) and extend to the outer limits of the arms in our images. Pitch angles are then determined from peaks in the Fourier spectra, as this is the most powerful method to find periodicity in a distribution (Considère & Athanassoula 1998; Garcia-Gomez & Athanassoula 1993). The radial range over which the Fourier analysis was performed was chosen by eye and is probably the dominant source of error in the calculation of pitch angles. As a result three different radial ranges (listed in Table 1) were chosen for each galaxy, and a mean pitch angle and standard error calculated for every object.

It should be noted that bars (often equipped with rather tight spiral arms outside the bar) form in heavy disks as a natural gravitational instability (Hohl 1971). However, unbarred spiral structure should be supported by dynamically light disks. The transition from light to heavy disks and

Figure 1. Greyscale images of the galaxies for which the FFT analysis was performed. The overlaid contours represent the FFT fit to the spiral structure.

the affect of this upon bar streangth is described by Bertin (1991) and Bertin & Lin (1996).

We are fully aware that the spiral arms in barred galaxies may depart from a logarithmic shape. The arms may break at a large angle to the bar and then wind back to the other side, as in a ‘pseudoring’. Outer pseudorings (e.g. NGC 3504) present additional complications, but we do wish to stress that our pitch angles always correspond to arm morphology outside of the inner bar/bulge or inner pseudoring region. The robustness of our method and the choice of radial range may be seen in the ringed SB(r) spiral NGC 5921, where our contours trace out two grand design stellar arms exterior to the bar and the inner ring (see Figure 3 in Block et. al. 2001).

The images were firstly deprojected to face-on. Mean uncertainties of position angle and inclination as a function of inclination were discussed by Considère & Athanassoula (1988). For a galaxy with low inclination, there are clearly greater uncertainties in assigning both a position angle and an accurate inclination. These uncertainties are discussed by Block et al. (1999), who took a galaxy with low inclination ($< 30^\circ$) and one with high inclination ($> 60^\circ$) and varied the inclination angle used in the correction to face-on. They found that for the galaxy with low inclination, that the measured pitch angle remained the same. However, the measured pitch angle for the galaxy with high inclination varied by $\pm 10\%$. Since we have only one object with an inclination angle $> 60^\circ$ in our sample (ESO 602 G25) and this object has an error $> 10\%$ on the pitch angle anyway, we assume that inclination affects are not a dominant source of error for these objects. It should also be noted that our deprojection assumes that spiral galaxy disks are intrinsically circular in nature.

Figure 1 shows the images of the spiral galaxies observed for this project, overlaid with contours representing the results of an inverse Fourier transform analysis of the $m=2$ component. After having deprojected the K band im-

ages and identifying the dominant modes, we calculated the inverse Fourier transform, as follows:

We define the variable $u = \ln r$. Then

$$S(u, \theta) = \Sigma_m S_m(u) \exp(im\theta) \quad (2)$$

where

$$S_m(u) = \frac{D}{\exp(2u)4\pi^2} \int_{-\infty}^{+\infty} G_m(p)A(p, m) \exp(ipu)dp \quad (3)$$

and

$$D = \Sigma_{i=1}^I \Sigma_{j=1}^J I_{ij}(u, \theta) \quad (4)$$

$G_m(p)$ is a high frequency filter used by Puerari & Dottori (1992). For the spiral with $\tan P = -\frac{m}{p_{max}^m}$ it has the form:

$$G_m(p) = \exp \left[-\frac{1}{2} \left(\frac{p - p_{max}^m}{25} \right)^2 \right] \quad (5)$$

where p_{max}^m is the value of p for which the amplitude of the Fourier coefficients for a given m is maximum. This filter is also used to smooth the $A(p, m)$ spectra at the interval ends (Puerari & Dottori 1992). The contour overlays of the inverse Fourier transform in Figure 1 indicate the excellent fit of our $m=2$ spiral modes to the spiral structure of the galaxies observed. The dust-penetrated arm classes and pitch angles are listed in Table 1.

4 ROTATION CURVE DATA

The 14 galaxies observed here all have H α rotation curve data measured by Mathewson et al. (1992). The rotation curves are presented in Figure 3. It should be noted that the rotation curves presented here are symmetrized rotation curves, obtained by averaging the measured values of rotation relative to the two opposite sides along the major axis.

As can be seen the rotation curves are of good quality. The errors on the data points in the rotation curves are a

Figure 2. Relative Strengths of spiral modes in the galaxies. Plots are in terms of phase versus relative amplitudes.

combination of the error intrinsic to the spectroscopic measurement, which Mathewson et al. (1992) quote as being $< 10 \text{ km s}^{-1}$, and the error associated with the procedure of folding the two sides of the galaxy, which is also typically $< 10 \text{ km s}^{-1}$. These rotation curves have been used to estimate the shear rates in these galaxies and more detail is given in the Discussion section of this paper.

The work presented by Block et al. (1999) consisted of only 4 galaxies. Here we present a spectroscopic/near-infrared imaging analysis of a further 14 galaxies. The rates of shear are derived from their rotation curves as follows

$$\frac{A}{\omega} = \frac{1}{2} \left(1 - \frac{R}{V} \frac{dV}{dR} \right) \quad (6)$$

where A is the first Oort Constant, ω is the angular velocity, and V is the velocity measured at radius R . The value A/ω gives the shear rate.

Using equation 6, we have calculated the shear rates for these galaxies, over the same radial ranges for which the Fourier analysis was performed and pitch angles calculated (the radial ranges are listed in Table 1). We selected several different radial ranges, just as in the Fourier analysis, and present mean shear rates and standard errors. The dominant source of error on the shear rate is the spectroscopic

Figure 3. Rotation curves from Mathewson et al. (1992).

errors given in the rotation curves (i.e. a combination of the intrinsic spectroscopic error and the error associated with folding the two sides of the galaxy). Typically speaking, this is $< 10\%$. These are listed in Table 1. In order to calculate the shear rate, the mean value of $\frac{dV}{dR}$ measured in $\text{km s}^{-1} \text{arcsec}^{-1}$ is calculated by fitting a line of constant gradient to the outer part of the rotation curve (i.e. past the radius of turnover). Average shear rates were then calculated for the rotation curve, over the radial ranges listed in Table 1. The shear rates listed in Table 1 are means of the three shear rates measured over the three radial ranges.

5 DISCUSSION

We now discuss the results for each galaxy individually:

ESO 515-G3: This galaxy is given a dust-penetrated class of $L\gamma$, due to its near-infrared pitch angle of $47.8^\circ \pm 0.7$ and its dominant $m = 1$ Fourier mode. It shows narrow $m = 1$ and $m = 2$ components in its Fourier spectra, with the $m = 2$ component also being very strong. The breadth of the Fourier components is indicative of the accuracy with which the observed spiral structure can be approximated by a logarithmic spiral. For broader Fourier components, a logarithmic spiral is less applicable. This galaxy has a rising rotation curve with a shear rate of 0.27 ± 0.01 .

ESO 574-G33: This galaxy is given a dust-penetrated class of $E\gamma$, due to its near-infrared pitch angle of $39.9^\circ \pm 1.0$ and its dominant $m = 2$ Fourier mode. It shows narrow $m = 1$ and $m = 2$ components in its Fourier spectra, with the $m = 1$ component also being very strong. It has a rising rotation curve with a shear rate of 0.37 ± 0.02 .

ESO 576-G51: This galaxy is given a dust-penetrated class of $E\beta$, due to its near-infrared pitch angle of $30.4^\circ \pm 1.9$ and its dominant $m = 2$ Fourier mode. It shows narrow $m = 1$ and $m = 2$ components in its Fourier spectra, with the $m = 1$ component also being very strong. Its rotation curve is approximately flat with a shear rate of 0.47 ± 0.04 .

ESO 583-G2: This galaxy is given a dust-penetrated class of $E\beta$, due to its near-infrared pitch angle of $28.4^\circ \pm 1.0$ and its dominant $m = 2$ Fourier mode. It shows a narrow $m = 2$ component in its Fourier spectra. Its rotation curve is approximately flat with a shear rate of 0.47 ± 0.04 .

ESO 583-G7: This galaxy is given a dust-penetrated class of $L\beta$, due to its near-infrared pitch angle of $17.7^\circ \pm 2.0$ and

its dominant $m = 1$ Fourier mode. It shows a narrow $m = 1$ component in its Fourier spectra. Its shear rate is 0.54 ± 0.02 and its rotation curve remains approximately flat.

ESO 602-G25: This galaxy is given a dust-penetrated class of $E\beta$, due to its near-infrared pitch angle of $21.8^\circ \pm 2.0$ and its dominant $m = 2$ Fourier mode. It shows a narrow $m = 2$ component in its Fourier spectra, and also a strong, but double-peaked $m = 1$ component. Its rotation curve is approximately flat with a shear rate of 0.45 ± 0.02 .

ESO 606-G11: This galaxy is given a dust-penetrated class of $H4 \beta$, due to its near-infrared pitch angle of $25.2^\circ \pm 2.4$ and its dominant $m = 4$ Fourier mode. It shows narrow $m = 1$ and $m = 4$ components and a double-peaked $m = 2$ component in its Fourier spectra, all of which appear as relatively strong modes. Its rotation curve is flat with a shear rate of 0.50 ± 0.03 .

IC 1330: This galaxy is given a dust-penetrated class of $E\gamma$, due to its near-infrared pitch angle of $37.8^\circ \pm 1.1$ and its dominant $m = 2$ Fourier mode. It shows a slightly broader than expected $m = 2$ mode, which may be due to confusion with the strong bar in this galaxy. Its rotation curve is rising with a shear rate of 0.35 ± 0.02 .

NGC 2584: This galaxy is given a dust-penetrated class of $E\beta$, due to its near-infrared pitch angle of $29.7^\circ \pm 3.0$ and its dominant $m = 2$ Fourier mode. It shows a narrow $m = 2$ mode, which is more than twice as strong as any other mode. Its rotation curve is flat with a shear rate of 0.50 ± 0.04 .

NGC 2722: This galaxy is given a dust-penetrated class of $H4\beta$, due to its near-infrared pitch angle of $32.8^\circ \pm 3.4$ and its dominant $m = 4$ Fourier mode. It shows a very broad modes from $m = 1$ to $m = 4$, which is probably due to the flocculent nature of its spiral structure, even when viewed in the near-infrared. Its rotation curve is approximately flat with a shear rate of 0.50 ± 0.03 .

NGC 3456: This galaxy is given a dust-penetrated class of $E\gamma$, due to its near-infrared pitch angle of $38.0^\circ \pm 0.6$ and its dominant $m = 2$ Fourier mode. It shows a very narrow $m = 2$ component, which is more than twice as strong as any other mode. Its rotation curve is rising with a shear rate of 0.31 ± 0.02 .

NGC 7677: This galaxy is given a dust-penetrated class of $E\alpha$, due to its near-infrared pitch angle of $17.0^\circ \pm 0.8$ and its dominant $m = 2$ Fourier mode. It shows a very narrow $m = 2$ component, which is more than three times as strong

Table 1. Results from the Fourier analysis and rotation curve analysis of 14 spiral galaxies. Column 1 shows the name of the galaxy; Column 2 shows the derived dust penetrated class; Column 3 shows the optically determined Hubble type; Column 4 shows the pitch angle for the $m=2$ component of the K-band spiral arms. The error associated with the pitch angle is related to the radial range over which the FFT is performed. The error is a standard error derived from the different pitch angles that are calculated when different radial ranges are used in the FFT analysis. The signal-to-noise ratio is probably the source of the error shown here. Column 5 shows the derived shear rate. The error associated with the shear rate is associated with the intrinsic spectroscopic error and the error associated with the procedure of folding the two sides of the galaxy. Column 6 shows the three radial ranges over which the pitch angle and shear rate were determined; Column 7 shows the position angle of the major-axis and column 8 shows the inclination angle to the plane of the sky.

Galaxy Name	Dust-penetrated class	Hubble Type	P_K	A/ω	Radial ranges in arcsec	Position angle	Inclination
ESO 515 G3	$L\gamma$	SB(rs)c	47.8 ± 0.7	0.27 ± 0.01	13.2-30.9; 12.3-31.8; 14.1-30.0	17°	48°
ESO 574 G33	$E\gamma$	SB(rs)bc	39.9 ± 1.0	0.37 ± 0.02	16.2-33.2; 15.3-34.1; 17.1-32.3	104°	49°
ESO 576 G51	$E\beta$	SB(s)bc	30.4 ± 1.9	0.47 ± 0.04	18.0-39.1; 18.0-40.0; 18.0-38.2	80°	46°
ESO 583 G2	$E\beta$	SB(rs)bc	28.4 ± 1.0	0.47 ± 0.04	10.0-27.8; 10.0-28.7; 10.0-26.9	52°	44°
ESO 583 G7	$L\beta$	SB(rs)c	17.7 ± 2.0	0.54 ± 0.02	16.8-36.4; 15.9-37.3; 17.7-35.5	40°	40°
ESO 602 G25	$L\beta$	SA(r)b	21.8 ± 2.0	0.45 ± 0.02	8.6-32.3; 7.7-33.2; 9.5-31.4	171°	62°
ESO 606 G11	$H4\beta$	SB(rs)bc	25.2 ± 2.4	0.50 ± 0.03	10.9-21.8; 10.0-22.7; 11.8-20.9	85°	46°
IC 1330	$E\gamma$	Sc? sp	37.8 ± 1.1	0.35 ± 0.02	18.0-27.3; 18.0-28.2; 18.0-26.4	60°	59°
NGC 2584	$E\beta$	SB(s)bc?	29.7 ± 3.0	0.50 ± 0.04	12.7-28.2; 11.8-29.1; 13.6-27.3	17°	57°
NGC 2722	$H4\beta$	SA(rs)bc	32.8 ± 3.4	0.46 ± 0.03	7.3-22.8; 6.4-23.7; 8.2-21.9	105°	49°
NGC 3456	$E\gamma$	SBc	38.0 ± 0.6	0.31 ± 0.02	7.7-25.5; 6.8-26.4; 8.6-24.6	80°	47°
NGC 7677	$E\alpha$	SAB(r)bc	17.0 ± 0.8	0.66 ± 0.02	20.0-37.8; 20.0-38.7; 20.0-36.9	35°	51°
UGC 14	$L\beta$	Sc+	20.9 ± 1.3	0.53 ± 0.03	8.2-20.5; 7.3-21.4; 9.1-19.6	32°	46°
UGC 210	$E\beta$	Sb	26.0 ± 0.8	0.55 ± 0.03	6.8-14.6; 5.9-15.5; 7.7-13.7	19°	60°

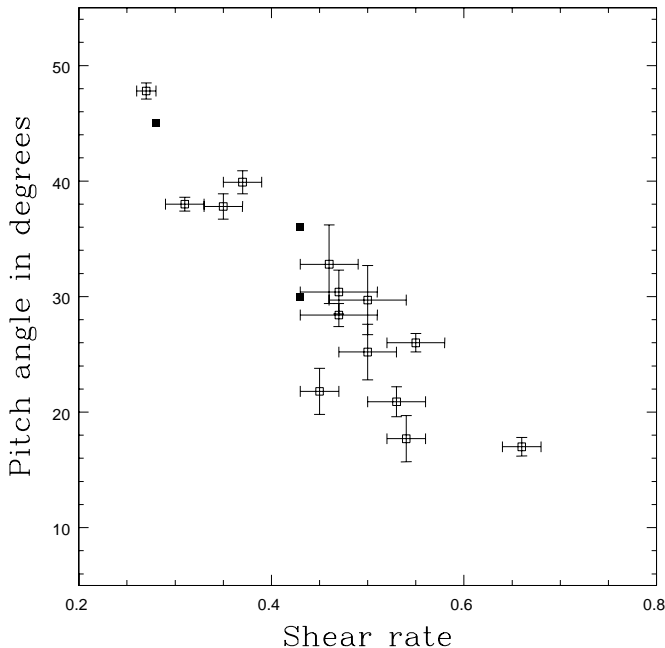


Figure 4. Near-infrared pitch angle in degrees versus shear rate. Hollow squares represent the 14 galaxies presented here. Solid squares are 3 galaxies presented in Block et al. (1999).

as any other mode. Its rotation curve is falling with a shear rate of 0.66 ± 0.02 .

UGC 14: This galaxy is given a dust-penetrated class of $L\beta$, due to its near-infrared pitch angle of $20.9^\circ\pm 1.3$ and its dominant $m = 1$ Fourier mode. It shows a narrow $m = 2$ component, with a double-peaked $m = 2$ mode. The double-

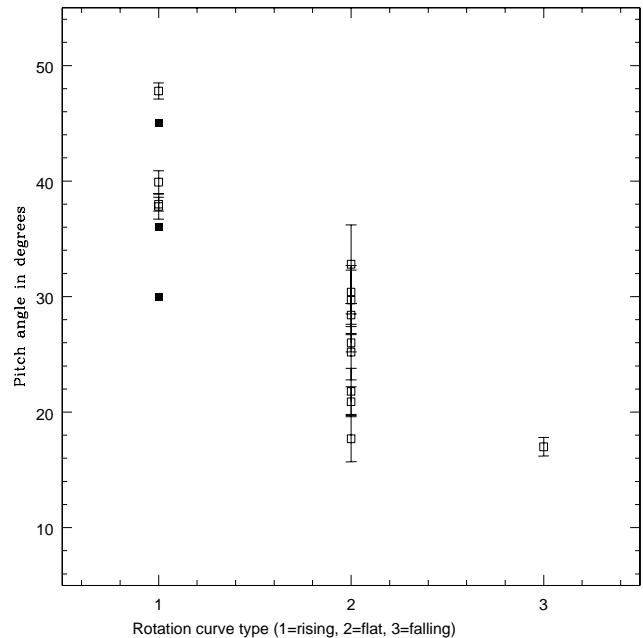


Figure 5. Near-infrared pitch angle in degrees versus rotation curve type. The symbols are the same as Figure 3

peaked $m = 2$ mode suggests that this galaxy has both a leading and a trailing $m = 2$ component. From the spectra, these components have very similar pitch angles, which explains why the error on the estimated pitch angle is still quite low. Its rotation curve has a shear rate of 0.53 ± 0.03 , due to its flat shape and this suggests a spiral of intermediate winding angle, as indicated by its dust-penetrated class.

UGC 210: This galaxy is given a dust-penetrated class of $E\beta$, due to its near-infrared pitch angle of $26.0^\circ \pm 0.8$ and its dominant $m = 2$ Fourier mode. It shows a narrow $m = 2$ component, with a secondary, but weaker peak. Its $m = 1$ component is also fairly strong. Its rotation curve remains approximately flat with a shear rate of 0.55 ± 0.03 .

Figure 4 shows a plot of the shear rate versus the near-infrared spiral arm pitch angle. As well as presenting a relatively tight correlation (correlation coefficient = 0.93; significance = 99.9%), it is also interesting to note how spiral galaxies seem to fall into 3 distinct areas on this plot, according to both their shear rates and their pitch angles. Galaxies with high shear rates (falling rotation curves) and tightly wound spiral structure are found in the bottom right and belong to the quantitative α bin in the dust penetrated class. Galaxies with shear rates of approximately 0.5 (flat) and intermediately wound spiral structure lie in the middle and belong to the β bin. Finally, the top left contains those galaxies with loosely wound structure and low rates of shear (associated with rising rotation curves). These spirals belong to the γ form family.

Figure 5 shows a plot between rotation curve type (Burstein & Rubin 1985), i.e. rising, flat or falling, versus spiral arm pitch angle. A tight correlation (wherein the correlation coefficient is 0.86 and the significance 99.9%) is found.

6 CONCLUSIONS

The shape of a rotation curve, beyond the turnover radius, is determined largely by the amount and distribution of matter (including dark matter) contained in a spiral galaxy. The increase of shear rates from low to high, dictates mass distributions from small to large central mass concentrations. The correlation found between pitch angle and shear rate is interpreted as follows: galaxies with higher rates of shear present a larger central mass concentration and more tightly wound arms. In contrast, open arm morphologies in the dust penetrated, near-infrared regime are associated with rising rotation curves, lower rates of galactic shear, and lower central mass concentrations. This correlation was alluded to by the pioneering work of Lin & Shu (1964) and by the later spectroscopic studies of Burstein & Rubin (1986). It is in agreement with modal theories of spiral structure (e.g. Bertin et al. 1989a, b; Bertin & Lin 1996) and other numerical models based on the modal theory (e.g. Fuchs 1991, 2000).

ACKNOWLEDGMENTS

The United Kingdom Infrared Telescope (UKIRT) is operated by the Joint Astronomy Centre on behalf of the U.K. Particle Physics and Astronomy Research Council (PPARC). DLB is indebted to Mrs M Keeton and the Board of Trustees of the Anglo American Chairman's Fund for their continued encouragement and support. This research utilized the NASA/IPAC Extragalactic Database (NED), operated by the Jet Propulsion Laboratory, California Institute of Technology, under contract with the National Aeronautics and Space Administration. The authors wish to thank

Paul Eskridge and George Lake for useful suggestions, and the anonymous referee for comments which greatly improved the content of this paper.

REFERENCES

- Bertin G., Lin C. C., Lowe S. A., Thurstans R. P., 1989a, *ApJ*, 338, 78
 Bertin G., Lin C. C., Lowe S. A., Thurstans R. P., 1989b, *ApJ*, 338, 104
 Bertin G., 1991, in *Dynamics of Galaxies and Their Molecular Cloud Distributions*, IAU 146, Kluwer, Dordrecht, p. 93
 Bertin G., 1993, *PASP*, 105, 640
 Bertin G., 1996, In *New Extragalactic Perspectives in the New South Africa*, eds Block D. L., Greenberg J. M., Kluwer, Dordrecht, p. 227
 Bertin G., Lin C. C., 1996, *Spiral Structure in Galaxies: A density wave theory*, MIT Press, Cambridge, MA
 Block D. L., Wainscoat R., 1991, *Nature*, 353, 48
 Block D. L., et al., 1994a, *A&A*, 288, 365
 Block D. L., et al., 1994b, *A&A*, 288, 383
 Block D. L., Elmegreen B. G., Wainscoat R. J., 1996, *Nature*, 381, 674
 Block D. L., Puerari I., 1999, *A&A*, 342, 627
 Block D. L., et al., 1999, *Ap&SS*, 269-270, 5
 Block D. L., Puerari I., Knapen J. H., Elmegreen B. G., Buta R., Stedman S., Elmegreen D. M., 2001, *A&A*, 375, 761
 Burstein D., Rubin V. C., 1985, *ApJ*, 297, 423
 Considère S., Athanassoula E., 1988, *A&AS*, 76, 365
 de Jong R. S., 1996, *A&A*, 313, 45
 Frogel J. A., Quillen A. C. Pogge, R. W., in *New Extragalactic Perspectives in the New South Africa*, eds D. L. Block, J. M. Greenberg, Kluwer, Dordrecht, p251
 Fuchs B., 1991, in *Dynamics of Disk Galaxies*, ed B. Sundelius, Chalmers University of Technology, p359
 Fuchs B., 2000, in *Galaxy Dynamics: From the Early Universe to the Present*, eds F. Combes & G. Mamon, ASP Conf. Ser. Vol. 197, p53
 Garcia-Gomez C., Athanassoula E., 1993, *A&AS*, 100, 431
 Hohl F., 1971, *ApJ*, 168, 343
 Hubble E. P., 1926, *ApJ*, 64, 321
 Kennicutt R. C. Jr., 1981, *AJ*, 86, 1847
 Lin C. C., 1971, in *Highlights of Astronomy Vol. 2*, ed. C. de Jager, Reidel, Dordrecht, p88
 Lin C. C., Shu F. H., 1964, *ApJ*, 140, 646
 Lindblad B., 1963, *Stockholm Obs. Ann.*, 5, 3
 Lynden-Bell D., Kalnajs A. J., 1972, *MNRAS*, 157, 1
 Mark J. W-K., 1971, *Proc. Natl. Acad. Sci.*, 68, 2095
 Martin P. G., Whittet D. G. B., 1990, *ApJ* 357, 113
 Mathewson D. S., Ford V. L., Buchhorn M., 1992, *ApJS*, 81, 413
 Pfenniger D., Martinet L., Combes F., 1996, in *New Extragalactic Perspectives in the New South Africa* eds D. L. Block, J. M. Greenberg, Kluwer, Dordrecht, p291
 Puerari I., Dottori H. A., 1992, *A&AS*, 93, 469
 Rhoads J. E., 1998, *AJ*, 115, 472
 Rix H.-W., Rieke M. J., 1993, *ApJ*, 481, 123
 Schröder M. F. S., Pastoriza M. G., Kepler S. O., Puerari I., 1994, *A&AS*, 108, 41

- Seigar M. S., James P. A., 1998, MNRAS, 299, 672
Seigar M. S., James P. A., 1998, MNRAS, 299, 685
Seigar M. S., Chorney N. E., James P. A., 2003, MNRAS,
342, 1
Thornley M. D., 1996, ApJ, 469, 45
Worthey G., 1994, ApJS, 95, 107

This figure "seigar_fig1a.jpg" is available in "jpg" format from:

<http://arxiv.org/ps/astro-ph/0502587v2>

This figure "seigar_fig1b.jpg" is available in "jpg" format from:

<http://arxiv.org/ps/astro-ph/0502587v2>

This figure "seigar_fig1c.jpg" is available in "jpg" format from:

<http://arxiv.org/ps/astro-ph/0502587v2>

This figure "seigar_fig2a.jpg" is available in "jpg" format from:

<http://arxiv.org/ps/astro-ph/0502587v2>

This figure "seigar_fig2b.jpg" is available in "jpg" format from:

<http://arxiv.org/ps/astro-ph/0502587v2>

This figure "seigar_fig3a.jpg" is available in "jpg" format from:

<http://arxiv.org/ps/astro-ph/0502587v2>

This figure "seigar_fig3b.jpg" is available in "jpg" format from:

<http://arxiv.org/ps/astro-ph/0502587v2>